

Detection to trace aluminum ion of pharmaceutical wastewater using synthesis of Schiff-based chemosensor

Mengistu Jemberu Dagnaw^{*} , Mahesh Gopal 

Department of Mechanical Engineering, Institute of Engineering and Technology, Wollega University, Post Box No.395, Nekemte, Ethiopia

Abstract

Background: The aim of this research was to develop a fluorogenic sensor for Al³⁺ ions, which have been identified as a possible food and drinking water pollutant by the WHO and considered to be harmful to human health.

Methods: The sensing mechanism was based on excited-state intramolecular proton transfer, with the intramolecular rotation restriction occurring after binding with the analyte. The probe attaches Al³⁺ selectively and emits strong emission in 4:1 H₂O/MeOH (v/v) solution while irradiated at 400 nm in the presence of a wide number of cations, acting as a "turn-on" fluorescence chemosensor. The range of detection for Al³⁺ is 3.3 nM (3 method), which is more than 200 times more responsive than the WHO suggested limit of 7.4 mM (3σ method). Mass spectra, job plot, and Benesi-Hildebrand plot were used to determine the formation of the 1:1 metal-to-ligand complex.

Results: Aluminum (Al) ion content in effluent obtained from the pharmaceutical sector is 0.381 mM, which is a trace amount. A separate in vitro experiment indicates that the probe can precisely perceive Al³⁺ ions in a cell line. The sensor-based method is developed to detect 3.3 nM of Al³⁺ ions, which is significantly less than the WHO max.

Conclusion: The probe to detect Al³⁺ ions in live cells. HL becomes a flexible sensor for recognizing intracellular Al³⁺ in human liver cancer cell line Hep G2 and human lung fibroblast cell lines by fluorescence cell imaging procedures, and the probe's non-toxicity has been proven by MTT tests up to 100M.

Keywords: Environment, Water, Pollution, Poisoning, Alzheimer's, Parkinson's dementia, Disease, Pharmaceutical, Aluminium, Fluorescence chemosensor, India

Citation: Jemberu Dagnaw M, Gopal M. Detection to trace aluminum ion of pharmaceutical wastewater using synthesis of Schiff-based chemosensor. Environmental Health Engineering and Management Journal 2021; 8(4): 309-318. doi: 10.34172/EHEM.2021.35.

Article History:

Received: 26 May 2021

Accepted: 11 July 2021

ePublished: 7 December 2021

*Correspondence to:

Mengistu Jemberu Dagnaw,
Email: mengejembe@gmail.com

Introduction

Aluminum (Al) is the most abundant metal on the planet's surface (8.3% of total metal mass). Al is released into the atmosphere as a consequence of the extraction and processing of ores, as well as the manufacture of Al wire, alloys, and chemicals. Fine Al particles in the air are either blown away by storms or fall to the ground. The quantity of pollution determines the toxicity of Al. Aluminium toxicity is mainly influenced by Al bioavailability, which is influenced by relatively low aluminium levels in natural sources, namely drinking water (1). Aluminium is a poisonous, insoluble, non-essential substance, which is present in most natural water that affects the human beings (2). However, acid rain, waste outflow, and soil extraction have all discharged significant amounts of Al into the atmosphere in recent years. The greatest concentration of Al in water supplies used as drinking water is 200 µg L⁻¹ (3). Since Al in drinking water was

largely made up of soluble species, as a result, it was thought that Al in drinking water will have a disproportionate impact on the Alzheimer's disease (AD) occurrence when it was consumed (4). The dialysis was performed to determine the amount of Al in muscle; the results revealed, that the average muscle contained 14.8 parts per million (PPM) of Al and the trabecular-bone contained 98.5 PPM. The uremic patient's traces are 25 ppm during dialysis, and the Al traces in the gray matter of the brain are greater in both patients (5). A higher incidence of dementia and AD has been associated with drinking water with high Al content (≥ 0.1 mg/L) (6). Martyn et al (7) conducted a research in different regions to find the presence of Al and silicon that causes the risk of AD in drinking water. The research showed that the higher Al and lower silicon concentrations in drinking water, increase the possibility of risk of AD at usual concentrations up to around 0.2 mg/L, and it was also



shown that drinking water with silicon contents more than 6 mg/L of molybdate-reactive silica seemed to have a protective effect. This research (8) used a random sample of 186 water utilities, with raw and completed water samples obtained five times over the course of a year and tested for iron and Al using the atomic absorption technique. Al is much almost certainly to be found in surface waters, only 9% of groundwaters contained visible levels of Al, while 78% of surface waters have detectable Al. The goal of this study was to assess the relationship between long-term exposure to different forms of Al in drinking water and the beginning of AD. The formation of AD has been associated with organic monomeric Al, which creates the illness. Compared to earlier research, this relationship was discovered in a geographic environment characterized by low Al quantities and high pH levels (9). Al levels over 80 g/L in drinking water has been related to an increased risk of AD. The findings of this study clearly suggest that metal such as Al in drinking water has no role in the etiology of senile dementia (10). McLachlan et al (11) reported that there is a possibility of Al concentration in drinking water which causes AD on the basis of strict neuropathologic criteria. The results of epidemiologic research, along with a broad body of laboratory evidence of Al neurotoxicity and elevated concentration of silicic acid (Si_2OH_4) would be in AD-affected brain, suggest that lowering and retaining appropriate residual Al in drinking water (at least below 100 $\mu\text{g}/\text{L}$) should be prioritized, particularly for older age groups at risk for AD. Al toxicity affects the plant growth but also affects the neurological system, producing diseases such as Alzheimer's and Parkinson's disease, and amyotrophic lateral sclerosis (12). Although the precise mechanism by which Al influences disease mechanisms remains unclear, there is an evidence that it increases oxidative stress and inflammatory events. These activities are also associated with AD and exposure to the metal may exacerbate the disease by enhancing these processes (13). Al fractions were measured in water samples collected from three water supply wells. All water treatment plants employed poly-Al chloride (PAC) as a coagulant; however, the Al-based coagulant had a minimal effect on the metal concentration of the raw water. Al concentrations in raw and treated water vary dramatically. More than 80% of Al in fresh water is in the form of particulates (14). The aim of this research was to determine the concentration of Al available in groundwater. Standard methods are used for the examination of water and wastewater to evaluate values of consistency factors such pH, turbidity, total dissolved solids (TDS), and Al content in 871 water samples (15). Simulated coil-pipe tests, batch reactor tests, and quartz crystal microbalance with dissipation monitoring were used to study the deposition characteristics of various Al species in PAC. Under stirring conditions, more Al may collect on the pipe surface for Al

species with a greater deposition tendency. For Al13 and Al30, the pH impact on deposition behavior was quite modest within the neutral pH range of 6.7–8.7 (16). This paper discusses the environmental and clinical tests are being used to determine the risk of disease. The aim of this study was to find out more about AD, breast cancer serving as a major endpoint. Internal Al load comparison levels (15 g/L in urine, 5 g/L in serum) are more likely to be exceeded in people who have been exposed to Al at work. The essential internal toxicity criteria for Al are found in blood and urine. For occupational exposure, the biological tolerance limit is 50 g of Al per gram of creatinine in the urine (17). The goal of this study was to determine the concentration of Al and cadmium (Cd) in cigarettes and drinking water. Electrothermal atomic absorption spectrometry was used to determine the quantities of Cd and Al in cigarettes, drinking water, and blood samples. The findings revealed that the levels of Al and Cd in lake and subterranean water were higher than the WHO-recommended safe drinking water limit (18). Drinking water with fluoride and Al is suspected to have harmful health consequences, particularly on the brain, liver, and kidneys. The levels of blood urea and creatinine were evaluated as indications of kidney malfunction. To determine the level of damage that the F, Al, and AlFx complex could produce, histopathological assessments of kidney tissues were performed (19). In this study, the unique low-cost defluoridation process based on coating Al hydroxide on the surface of rice husk ash. Rice husk ash is made by burning rice/paddy husk, which is a readily available and low-cost raw material. The adsorption capacity was determined to be between 9 and 10 mg/g, indicating high fluoride removal effectiveness (20). The present study contains a number of statistical benefits, such as the study size and prospective breadth, as well as well-defined illness diagnoses. Individual socio-demographic characteristics, as well as data on other important drinking water factors were analyzed to find out whether these factors may be confusing for the association between Al and AD (21). The main cause of Al effects on the water distribution system and human health is its speciation in drinking water. To reduce Al bioavailability in drinking water, orthophosphate should be added before the coagulant process, and fluoride and silicic acid concentrations should be kept below 2.0 and 25 mg/L (22). The impact of PAC coagulant qualities on soluble residual Al concentrations following coagulation and filtration was investigated in this study. While by increasing the dose of normal-basicity, the polyaluminum chloride (PACls) increased the dissolved residual Al concentration at pH 7.5, raising the dosage of high-basicity PACls decreased the soluble residual Al concentration at pH 7.5. The capacity of high-basicity PACls to minimize residual Al concentrations was maintained at higher raw water temperatures, despite the

fact that residual Al concentrations was maintained (23). Maximum contaminant guidelines are utilized to limit pollutants in drinking water in order to prevent health problems. Al-induced bone disease may cause stress fractures in the ribs, femur, vertebrae, humerus, and metatarsals. Serum Al $\geq 100 \mu\text{g/L}$ has a 75%–88% positive predictive value for Al bone disease. The preterm infants, infants with congenital uremia, and children and adults with kidney disease are all at increased risk of systemic Al poisoning following repeated intake of monomeric Al salts (24). Al has been hypothesized to have a role in the development of AD. Although the precise mechanism of Al toxicity is unknown, growing evidence indicates that the metal may enhance oxidative and inductive reactions, ultimately leading to tissue damage. This study examines Al overall toxicity, with a focus on the ways through which it may hasten the development of chronic age-related neurodegenerative diseases (25). Pharmaceutical manufacturing plants contaminate plants, humans, and animals directly. The Organization for Economic Co-operation and Development (OECD) is now encouraging countries to decrease pharmaceutical production; nevertheless, the UK, Germany, and other countries that depend on pharmaceutical products for income, are reportedly still manufacturing a significant quantity of medicines (26). Large amounts of pharmaceuticals are utilized, resulting in increasing discharge into the environment. Medicines are designed to resist photodegradation, biodegradation, and chemical breakdown until they are injected and perform particular pharmacological activities; residual pharmaceutical chemicals are handled with normal water/wastewater treatment (27). In the aquatic environment, pharmaceuticals and drug metabolites have been found. Under certain recharge conditions, polar pharmaceutically active compounds (PhACs) such as clofibrate acid, carbamazepine, primidone, or iodinated contrast agents may leak into groundwater aquifers. Most active medications are removed through metabolism and urine after being eaten, and PhACs have been discovered in groundwater contaminated by landfill leachates or industrial leftovers (28).

In several nations, pharmaceutical medications have been discovered in small amounts in sewage treatment plant effluents, surface waters, seawaters, groundwater, and some drinking waters. The effects of various medications on aquatic animals have been studied using acute toxicity testing. It was reported that in surface water concentrations are lower and so there is low environmental risks (29). In 2015, the global pharmaceutical business was valued US\$1.06 trillion, with an annual average growth rate of 5.2%. According to estimates, North America's trade is valued US\$363.2 billion, Europe's is worth USD 315.1 billion, and Asia's market is worth US\$281.3 billion. As the pharmaceutical industrial sector in South Korea is

rapidly increasing, there is an increase in people suffering from chronic diseases. With a 5-year average annual growth rate of 2.1%, its gross pharmaceutical production increased by 3.4% in 2015, reaching KRW 16969.6 billion. The pharmaceutical industry is projected to continue to expand rapidly over the next five years (30). Artificial neural network models and multivariate regression models were used to study the influent characteristics of water that are measured in the Birjand Waste Stabilization Pond (WSP) in Iran, such as pH, chemical oxygen demand, biological oxygen demand over 5 days (BOD₅), total suspended solids, total dissolved solid (TDS), Electrical conductivity (EC) and turbidity , and turbidity. The pseudo-first kinetics and the Langmuir-Hinshelwood model is used to determine the extent of degradation process and the removal of p-Nitroaniline (PNA) from aqueous solutions using novel semi-fluid Fe/charcoal reactor. The optimization is carried out to determine the halfway and final products in degradation reaction path (31). Khodadadi et al (32) found that TDS is considered as the most descriptive characteristic of influent wastewater to predict the WSP performance. Seven residue samples were collected from completely different locations and depths of the watercourse. The texture, clay, extractable iron and organic content of the sediments were measured. Pyrolysis-gas chromatography activity, mass spectrometry analysis showed that there are 3 types of organic substances: Crude hydrocarbons, artificial, and plant residues (33). Malakootian et al conducted a study to remove acid red 18 dye contained in wastewater, which are untreated in the aqueous environment, using hybrid micro-electrolysis process, including iron and Charcoal under the influence of ultrasonic waves (Fe/C/US) (34). The parameters affecting the adsorption process such as initial pH solution, adsorbent concentration, CIP concentration, and contact time are considered for experimental study. Fe₃O₄@ SiO₂-Schiff base nanocomposite (Fe₃O₄@ SiO₂-APTMS-HBA) was synthesized in in this study. The results showed that the maximum removal efficiency rate is 96% under the optimum process conditions (pH = 7, contact time = 5 min, CIP concentration = 10 mg/L, and adsorbent concentration = 50 mg/L) (35). Al is not a biological metal that is stored in the tissues comprising nerve cells. Nerve cell transmission would be inhibited or disrupted if insoluble Al-salts are deposited. As a result, biological communication, information transfer, and other aspects of human life are severely disrupted, resulting in Al-related bone diseases, encephalopathy, myopathy, and various neurodegenerative diseases such as AD, Parkinson's dementia, and other neurodegenerative diseases in the human body. With the increased use of Al, it is possible the plant roots would be harmed.

In this study, a synthesized probe 1-(1-(Phenyl (pyridine-2-yl) methyl)-1H-benzo[d]imidazol-2-yl) naphthalene-2-ol was designed for the selective and

sensitive detection of Al^{3+} in semi-aqueous media. During complication with CH_3CN , there is no proton conversion. In Hep G2 cells, the fluorescence specific concentration of HL in the presence of multiple anions, as well as the intracellular detection of Al^{3+} ion, was investigated.

Materials and Methods

Raw materials

All reagents and solvents used for synthesis were purchased from commercial sources and used as received. The chemicals and solvents were used in synthesis. Milli-Q water was used to render both aqueous solutions (Millipore). 2-hydroxy-1-naphthaldehyde (HNA) was purchased from Merck (Germany), and $\text{Al}(\text{NO}_3)_3 \cdot 9\text{H}_2\text{O}$ and Merckoglas were purchased from Merck, (Darmstadt, Germany). N^1 -(Phenyl (pyridine-2-yl) methyl) benzene-1, 2-diamine was synthesized using the previously mentioned method (36). All extra solutions and chemicals (AR grade) were purchased from Merck and finally used without further purification.

Instruments used

UV-VIS spectra were obtained using a Perkin Elmer Lambda 25 spectrophotometer, fluorescence spectra were obtained using a Perkin Elmer Spectro fluorometer type LS55, and FT-IR spectra (KBr disc, 4000–400 cm^{-1}) using a Perkin Elmer LX-1FTIR spectrophotometer. TMS was used as an internal standard to achieve NMR spectra on a Bruker (AC) 500 MHz NMR spectrometer. Water HRMS model XEVO-G2QTOF#YCA351 spectrometer was used to record ESI mass spectra. Both tests were performed at room temperature. The melting point was measured in an open-mouth capillary using a hot-plate melting point apparatus.

Synthetic procedures and formulation of the probe

The chemosensor was made by combining N^1 -(Phenyl(pyridine-2-yl)methyl)benzene-1, 2-diamine (0.273 g, 1.0 mmol), and 2-hydroxy-1-naphthaldehyde (0.172 g, 1.0 mmol) in MeOH (15 mL) under stirring for 12 hours at room temperature to produce the probe 1-(1-(Phenyl(pyridine-2-yl)methyl)benzyl)naphthaldehyde-2-ol(1H-benzo[d]imidazole-2-yl)naphthaldehyde-2-ol. The solvent was extracted after ensuring that there was no additional amine and enabling the MeOH solution of the probe to slowly evaporate. The crude substance was eventually filtered using paper chromatography, yielding needle-shaped red crystals. Mass spectrometry revealed a molecular ion peak that is higher than the predicted one. However, the simplest explanation is to consider the complication of the solvent, acetonitrile (CH_3CN), with these Al^{3+} ions.

Synthesis of aluminum-complex

The Al^{3+} complex of the chemosensor was made by combining a refluxing MeOH (10 mL) solution of

$\text{Al}(\text{NO}_3)_3 \cdot 9\text{H}_2\text{O}$ (0.375 g, 1 mmol) with a MeOH (10 mL) solution of the chemosensor (1 mmol, 0.427 g), and stirring the mixture for 12 hours to produce an orange solution. The solvent was extracted from the solution after allowing it to evaporate. The result was an orange-colored rigid mass.

Spectroscopic studies

A general method for UV-VIS and fluorescence studies

The probe (2.14 mg, 0.001 mmol) was soluble in MeOH (5 mL) and 100 μL of HL solution was diluted with 2 ml MeOH-H₂O (v/v 1:4) to give a cumulative volume of 2.1 mL. In water 10 mL of $\text{Al}(\text{NO}_3)_3 \cdot 9\text{H}_2\text{O}$ (3.75 mg, 0.001 mmol) was dissolved. The Al^{3+} solution (100 μL) was added to the HL solution predefined sequence. This sample solution preparation technique may also be used with other cations. At room temperature, the spectra were registered after mixing. The excitation wavelength for the fluorescence sample was 400 nm (excitation slit = 10.0 and emission slit = 7.0).

Calculation of the chemosensor's fluorescence quantum yield (Φ) before and after the Al^{3+} complication

The following equation was used to calculate the fluorescence quantum yield of the chemosensor and the metal-complex (37).

$$\Phi_{\text{sample}} = (\text{OD}_{\text{std}} \times A_{\text{sample}}) / (\text{OD}_{\text{sample}} \times A_{\text{std}}) \times \Phi_{\text{std}} \quad (1)$$

Where, A_{sample} and A_{std} represent the areas under the fluorescence spectral curves of the sample and standard sample.

And $\text{OD}_{\text{sample}}$ and OD_{std} are the optical densities of the sample and standard designated at the excitation wavelength.

Acidic quinine sulfate was taken as the standard ($\Phi_{\text{std}} = 0.54$) for the quantum yield calculation of ligand and Al complex.

Live cell imaging

Cell line culture

Cell line from a human liver cancer patient from the National Center for Cell Science (NCCS) in Pune, India, provided Hep G2 and human lung fibroblast cells, WI38. The cells were developed at 37°C and 5% CO_2 in DMEM with 10% FBS (fetal bovine serum), penicillin/streptomycin (100 units/mL), and penicillin/streptomycin (100 units/mL). All of the treatments were carried out at 37°C with a cell density allowed for exponential development (38).

Cell imaging

Hep G2 cells were cultured on coverslips for 24 hours. After that, the cells were either mock-treated or treated with 5 μM ligand and 10M Al^{3+} salt for 24 hours at 37°C.

Before being viewed under a fluorescence microscope, the cells were rinsed in 1× PBS and put on a glass slide (Leica).

Cell survivability assay

The probe's cell survival was investigated in human lung fibroblast cells, WI38, using a technique described by Samui et al (39). In a nutshell, the MTT test was used to determine the vitality of WI38 cells following exposure to various doses of ligand. The cells were seeded at 10⁴ cells per well in 96-well plates and subjected to the probe at concentrations of 0, 20, 40, 60, 80, and 100 µM for 24 hours. After treatment, cells were washed twice with 1PBS and incubated for 3-4 hours at 37°C with MTT solution (450 µg/mL). After dissolving the formazan crystals in MTT solubilization solution, the solution was read at 570 nm with a spectrophotometer (BioTek) and matched to control cells.

Synthesis of aluminum-complex

Micro analytical data

The Al³⁺-complex of the chemosensor was generated by combining a MeOH (10 mL) solution of the chemosensor (1 mmol, 0.427 g) with a refluxing MeOH (10 mL) solution of Al(NO₃)₃.9H₂O (0.375 g, 1 mmol) and stirring for 12 hours to produce an orange solution. The substance was permitted to evaporate, and the solvent was separated from the solution as a result of the evaporation. Finally, a strong mass of orange pigment was collected.

Spectroscopic studies

A broad approach to UV-VIS and fluorescence research

Al³⁺-complex of the chemosensor was generated by combining a MeOH (10 mL) solution of the chemosensor (1 mmol, 0.427 g) with a refluxing MeOH (10 mL) solution of Al(NO₃)₃.9H₂O (0.375 g, 0.001 mmol) and whole mixture was stirred for 12 hours to produce an orange solution. The substance was permitted to evaporate, and the solvent was separated from the solution as a result of the evaporation. Finally, a strong mass of orange pigment was collected.

Results

The probe's synthesis and formulation

The condensation of N¹-(Phenyl (pyridine-2-yl) methyl) benzene-1,2-diamine and 2-hydroxy-1-naphthaldehyde generated 1-(1-(Phenyl(pyridine-2-yl)methyl)benzene-1,2-diamine-1H-benzo[d]imidazol-2-yl) naphthalene-2-ol with a strong yield of 84% and a melting point of 190°C. It was characterized by spectroscopic measurements. The determined molecular weight of 428.1685 and the molecular ion peak of (HL + H)⁺ endorse the molecular identification. The weak bands at 3360 and 3070 cm⁻¹ belong to ν(phenolic-OH) and ν(-NH), respectively. ν(-CH=N-) stretching is associated with strong stretches at 1620 cm⁻¹. The singlet at 15.12 ppm correlates to δ(phenolic-OH); benzylic-H (CH-N) at 9.73 ppm in the

1H NMR range of HL (500 MHz, DMSO-d₆). At 5.90-8.64 ppm, other aromatic protons may be found.

Measured and experimentally micro analytical data

The measured and experimentally defined values for the probe (C₂₉H₂₁N₃O) were C, 81.48 (81.11) percent; H, 4.95 (5.05) percent; and N, 9.83 (9.81) percent, respectively. 1H NMR (500 MHz, DMSO-d₆): 15.12 (s, 1H, OH), 9.73 (s, 1H, benzylic-H), 5.90-8.64 (aromatic-H), IR: 3360 cm⁻¹ (Phenolic-OH), 3070 cm⁻¹ (-NH). No doubt this is N-H because Nitrogen has quadrupole moment and that would give rise to broadening, 1620 cm⁻¹ (imine - CH=N-). ESI-MS shows Molecular peak at 428.1641 for [HL + H]⁺(Mol.wt.(calculated), 428.1685) and at 450.0438 for [HL + Na]⁺(Mol.wt. Calculated=450.17).

Diffractive X-ray structure of the probe

Table 1 shows the monoclinic system of space group P 21/c for the red X-ray diffraction.

Table 1 shows the ligand's crystallographic information as well as structure refinement parameters. It also shows the acyclic structure of the probe. The reaction of HL with Al(NO₃)₃.9H₂O in methanol produced [Al(CH₃CN)]²⁺, a mononuclear Al-complex. The complex has no large peaks at 3360 cm⁻¹ and 3070 cm⁻¹, indicating the absence of -OH and -NH stretching, and (-CH=N-) at 1625 cm⁻¹, indicating a higher energy than HL. A molecular ion peak at 495.16 is visible in the mass spectrum, which could be the result of AlL(CH₃CN) + H⁺. During synthesis, the absence of (phenolic-OH) and -NH facilitates probe

Table 1. Crystallographic data and structure refinement parameters of the ligand

Formula	HL (ligand)
Empirical formula	C ₂₉ H ₂₁ N ₃ O
Formula weight	429.50
Crystal System	Monoclinic
Space group	P 2 ₁ /c
a (Å)	22.180(3)
b (Å)	5.9098(7)
c (Å)	16.938(2)
α= γ /°	90
β/°	94.383(4)
V (Å) ³	2213.7 (5)
Z	4
D _c /g cm ⁻³	1.289
μ/mm ⁻¹	0.079
λ(Å)	0.71073
Data [<i>I</i> >2σ (<i>I</i>)] / parameter	3882/299
GOF ^c	1.138
Final R indices [<i>I</i> >2σ(<i>I</i>)] ^{a,b}	R ₁ =0.0913, wR ₂ =0.1730

ionization and Al³⁺binding.

Synthesis of Al-complex

Micro analytical data of the Al³⁺ complex

Figure 3 shows the micro analytical data of the Al³⁺ complex ($C_{31}H_{25}AlN_4O_1$) with calculated values (%) of C, 75.29; H, 4.69; N, 11.33; IR: 1625 cm⁻¹ (imine -CH=N-). For [AlL (CH₃CN)]²⁺ + H⁺, M, the mass spectrum reveals a strong peak at 495.19 and showed the weight of 495.16.

UV-VIS spectroscopy experiments

At 25°C, spectrophotometric titrations of HL in 1:4 MeOH/H₂O (v/v) with progressive additions of Al³⁺ were used to explore the interaction of HL with Al³⁺. The probe's absorption maxima are initially 428 nm, but after association with the Al³⁺ ion, the absorbance increases with a slight red shift of the maximum to 438 nm (Figure 1), demonstrating that the reaction is clean and uncomplicated. Intramolecular charge transfer through chelation is responsible for the red-shifting of the HL bands generated by Al³⁺inclusion. The increase in absorbance is linear until the molar ratio of [Al³⁺]:[HL] reaches 1:1, at which it becomes non-variable as [Al³⁺] increases. It indicates that HL and Al³⁺have a stoichiometry of 1:1. The job plot was created by scheming the absorbance versus various mole fractions of Al³⁺while keeping the volume of the solution constant, and the molar fraction maxima were achieved at roughly 0.5-mole fraction, which supported 1:1 complex formation of HL and Al³⁺.

Fluorescence sensing for Al³⁺

The fluorescence quantum yield was estimated using quinine sulfate as a reference and a standard of MeOH/H₂O (v/v 1:4) with a known quantum yield of R= 0.54 (40). When the probe was excited at 400 nm, no emission was recorded. The ligand and quinine sulfate ($C_{40}H_{50}N_4O_8S$) were stimulated at the same wavelength (502 nm), and their absorbance was almost identical. As a result, the ligand's quantum yield (Φ_{ligand}) was 0.0186, and following chelation with Al³⁺, the high-intensity emission band at 502 nm was detected. As a consequence, the calculated quantum yield for the Al³⁺-complex is 0.2748. As a consequence of the metal complication, the fluorescence quantum yield raised.

As a result of the metal complication, the fluorescence quantum yield increases. Other cations (Na⁺, K⁺, Ca²⁺, Mg²⁺, Mn²⁺, Fe³⁺, Zn²⁺, Co²⁺, Ni²⁺, Pd²⁺, Cd²⁺, Hg²⁺, Cu²⁺, Ba²⁺, and Pb²⁺) have negligible fluorescence emission in MeOH/H₂O (v/v 1:4). As a consequence, under comparable experimental settings, the probe preferentially shows "turn on" Al³⁺emission (Figure 2). The fluorescence intensity increases with the constant addition of Al³⁺to the probe solution until it reaches a 1:1 molar ratio, at which point it becomes saturated. When Al³⁺is abundantly added to the mixture, the rate of

emission does not change (Figure 3).

Drawing of job plot by fluorescence spectroscopy method

The increase in fluorescence strength for HL + Al³⁺ may be attributed to the reduction of ESIPT in free HL and the chelation enhancement effect induced by the coordination of the ligand's -O and -N donor sites with the metal ion.

The binding constant value of Al³⁺with the probe was measured using the modified Benesi-Hildebrand equation, $1/\Delta F = 1/\Delta F_{\max} + (1/K[C]) (1/\Delta F_{\max})$. $\Delta F = F - F_0$ and $\Delta F_{\max} = F_{\max} - F_0$, where F_0 , F , and F_{\max} are the fluorescence emission intensities of the probe in the absence of Al³⁺, at an intermediate Al³⁺concentration, and at a concentration of total saturation, respectively, where K is the binding constant and $[C]$ is the Al³⁺concentration. The slope of the plot of $(F_{\max} - F_0)/(F - F_0)$ against $[C]^{-1}$ for the probe was used to calculate the value of K .

To obtain a deeper understanding of the complexation reaction, a fluorometric titration was conducted, and the relationship $[(F_{\max} - F_0)/(F - F_0)]$ versus $1/[Al^{3+}]$ was plotted using the Benesi-Hildebrand equation (Figure 4), and the

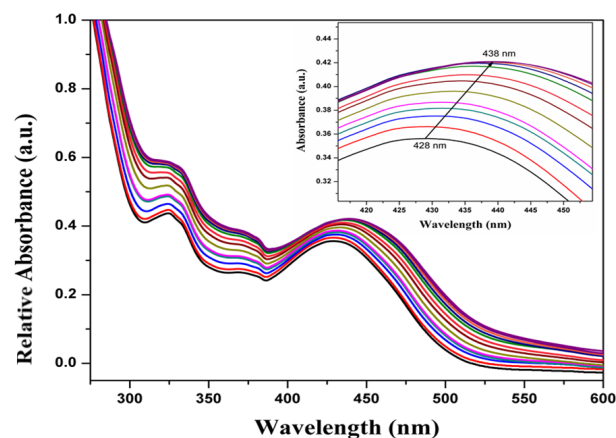


Figure 1. Change in HL (50 μ M) absorption spectrum with gradual addition of Al³⁺ions (5 μ M each) in MeOH/H₂O (v/v 1:4); inset: zoom picture at wavelength of 415–455 nm.

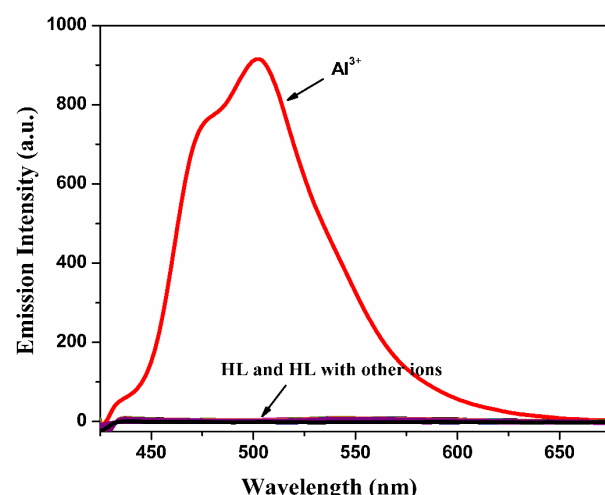


Figure 2. Change in emission spectrum of HL (50 μ M) upon gradual addition of different metal ions (100 μ M each) in MeOH/H₂O (v/v 1:4).

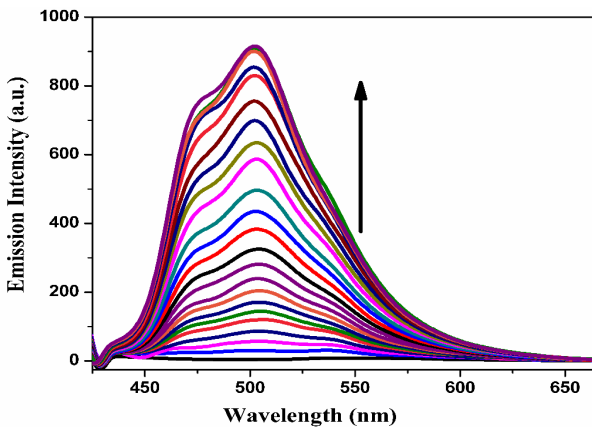


Figure 3. Changes in the emission range of HL (50 μM) varies when Al^{3+} ions (5 μM each) are progressively introduced to $\text{MeOH}/\text{H}_2\text{O}$ (v/v 1:4).

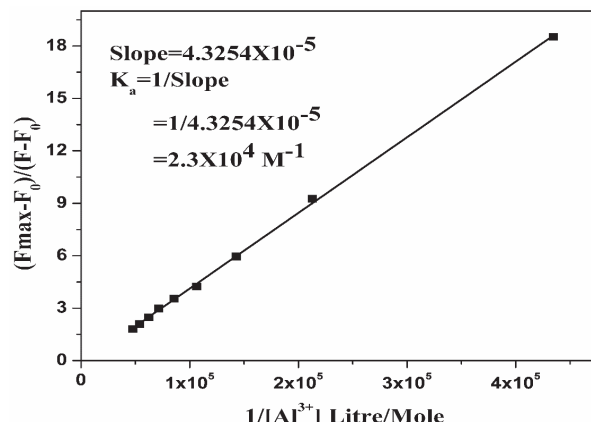


Figure 4. Benesi-Hildebrand plot of $\{(F_{\text{max}} - F_0)/(F - F_0)\}$ vs. $1/[\text{Al}^{3+}]$ by fluorescence spectroscopy-fluorescence titration curve of the ligand with Al^{3+} .

interaction constant (K_a) calculated by the fluorescence titration method for ligand with Al^{3+} was found to be $2.3 \times 10^4 \text{ M}^{-1}$. Following the 3σ process, the maximum of detection of Al^{3+} was determined to be 3.3 nM.

The effect of pH on the fluorescence strength of HL and the HL- Al^{3+} complex was investigated; it was discovered that HL emits no significant fluorescence in the pH ranges of 2 to 12, and that the ligand emits in pH ranges of 6.0 to 12 when Al^{3+} is present, as shown in Figure 5. In the pH range of 2–12, the probe is stable, with a maximal turn-on response to Al^{3+} at pH 6. The intensity of the emission drops sharply at pH 7, which might be due to the combination of bases with a metal ion (Al^{3+}), which reduces the ligand-metal interaction. This means that the HL will detect Al^{3+} in biological pH at far lower quantities than the WHO recommended value (7.41 mM) in drinking water.

For the detection of Al^{3+} , intervention on fluorescence by various citations has been studied. Figure 6 shows that no significant interference is observed.

Fluorescence lifespan estimates were used to estimate the reliability of the stimulated probe and its Al complex. Figure 7 exhibits bi-exponential ($\tau_{av} = 0.3290 \text{ ns}$) and mono-exponential ($\tau = 3.4637 \text{ ns}$) fluorescence decay profiles for

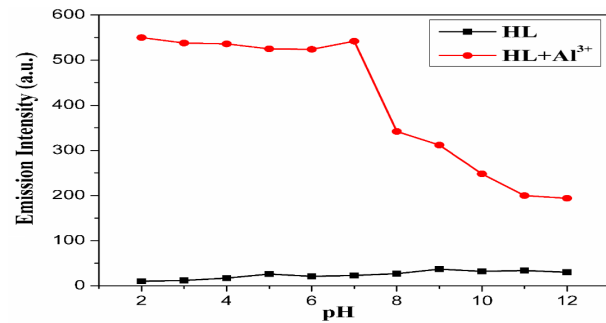


Figure 5. Fluorescence intensity of the receptor HL and the HL- Al^{3+} combination as a function of pH.

the ligand and its Al complex, respectively. The longer lifespan of the complex for ligand might be due to the increased stability of the complex in an excited state.

Here, the sensitivity of highly emissive Al complex with different anions like $\text{S}_2\text{O}_3^{2-}$, SCN^- , PO_4^{3-} , H_2PO_4^- , HPO_4^{2-} , I^- , OAc^- , ClO_4^- , SO_4^{2-} , HSO_4^- , Cl^- , F^- , HF_2^- , NO_3^- , Br^- , NO_2^- , CN^- , N_3^- , AsO_4^{3-} , and AsO_2^- was checked, and it was found that some of the anions (PO_4^{3-} , H_2PO_4^- , HPO_4^{2-} , F^- , and HF_2^-) quench the emission i.e., it is not specific for a single anion, as shown in Figure 8.

Detection of Al^{3+} ion in industrial wastewater

The industrial waste water (200 m³) by the direct application in chemosensor for the detection of Al^{3+} ion was studied. The fluorescence concentration is calculated

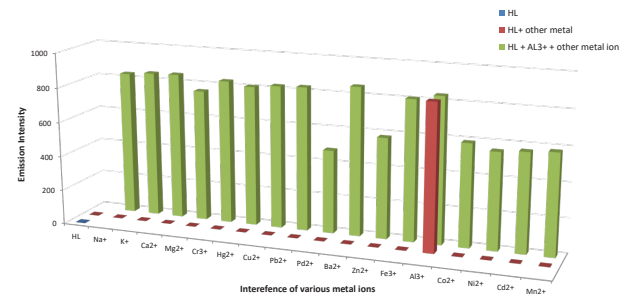


Figure 6. Interference of other metal ions towards Al^{3+} ion sensitivity.

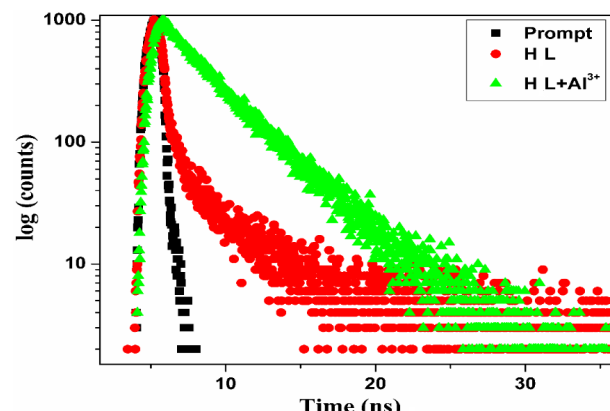


Figure 7. Fluorescence lifetime plot of the probe and Al complex in $\text{MeOH}/\text{H}_2\text{O}$ (v/v 1:4).

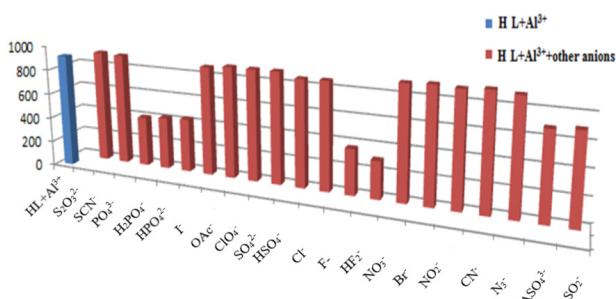


Figure 8. Change in emission intensity of the emissive Al-complex with different anions.

at 502 nm emission on excitation at 400 nm to produce a calculation plot by volume of analyte (Al^{3+}) and emission intensity (a.u.) in a 1:4 MeOH/H₂O (v/v) medium. The wastewater samples (200 mL) were collected from the pharmaceutical sector in Kolkata, West Bengal, India, in a clean and PVC container. The calibration plot was used to determine the unknown quantity of Al^{3+} in the collected wastewater sample, and the quantity of Al^{3+} is presented in Table 2.

The emission intensity changes linearly as the concentration of Al^{3+} ion-containing effluent increases, and no regression was performed.

Living cell imaging

Cell survivability assay to determine its biocompatibility

The probe in vitro cytotoxicity was assessed on the WI-38 cell line to determine its biocompatibility. The MTT test was done after the cells were treated for 24 hours with five different doses of ligand (20, 40, 60, 80, and 100 μM). At a maximum concentration of 100 μM , the ligand showed no significant toxicity. As a result, the ligand is biocompatible and suited for biological applications.

Fluorescence microscopic examination of cell imaging

The fluorescence microscopic examination was carried out to visualize the cellular absorption of the probe (5 μM) and Al^{3+} salts (10 μM). Under the microscope, a clear blue fluorescent light could be detected. Based on this finding, it can be deduced that the cells readily absorb the probe and the Al^{3+} salts, resulting in a blue fluorescent signal. As a result, the probe was successfully used to identify intracellular Al^{3+} in HePG2.

Discussion

Pharmaceuticals Al has been tested and developed as a fluorogenic sensor for Al^{3+} ions, which have been identified as a possible food and drinking water pollutant.

The detection of Al^{3+} ions is very important because it can cause human liver cancer and human lung fibroblast. The main aim of the study was to design a fluorescent chemosensor (41) and investigate detection trace Al^{3+} ions from pharmaceutical wastewater. The molecular ion peak of $(\text{HL} + \text{H})^+$ was 428.1641 and the calculated molecular weight was 428.1685 g/mol, which supports the molecular identity. The weak band at 3360 and 3070 cm^{-1} refer to (phenolic-OH) and (-NH), respectively. Strong stretches at 1620 cm^{-1} are assigned to (-CH=N-) stretching. The 1H NMR spectrum of HL (500 MHz, DMSO-d₆) demonstrates singlet at 15.12 ppm corresponds to δ (phenolic-OH); benzylic-H (CH-N) at 9.73 ppm. Other aromatic protons appear at 5.90-8.64 ppm. The probe has absorption maxima at 428 nm, but upon coordination with Al^{3+} ion, there is an increase in absorption with a small red shift of the maxima to 438 nm, indicating that the reaction is clean and straightforward. The red-shifting of the bands of HL (ligand) upon Al^{3+} addition is attributed to an intramolecular charge transfer through the chelation. The change of absorbance is linear until the molar ratio $[\text{Al}^{3+}]:[\text{HL}]$ reaches 1:1, as well as no longer changes with an increase in $[\text{Al}^{3+}]$. It suggests that the stoichiometry between HL and Al^{3+} is 1:1. The fluorescence emission of HL with other cations (Na^+ , K^+ , Ca^{2+} , Mg^{2+} , Mn^{2+} , Fe^{3+} , Zn^{2+} , Co^{2+} , Ni^{2+} , Pd^{2+} , Cd^{2+} , Hg^{2+} , Cu^{2+} , Ba^{2+} , and Pb^{2+}) in MeOH/H₂O (v/v 1:4) is insignificant. Thus, the probe is selectively showing “turn on” emission to Al^{3+} under the identical experimental condition. The probe is stable in the pH range of 2–12, and the maximum turn-on response to Al^{3+} was observed at pH 6. At pH 7, there was a sudden decrease in emission intensity; this might be due to the interaction of bases with a metal ion (Al^{3+}) and lower the ligand-metal interaction. This indicates that the HL is useful for the detection of Al^{3+} at the biological pH at a much lower concentration than that of the WHO recommended value (7.41 mM) in drinking water. For binding stoichiometry of HL and Al^{3+} , the molar fraction maxima were obtained at around 0.5 mole fraction, which indeed supports 1:1 complex formation of HL and Al^{3+} . The ligand exhibited no significant toxicities even at the highest concentration of 100 μM . Therefore, the ligand is good biocompatible and is beneficial for biological applications.

Conclusion

The condensation reaction of N¹-(Phenyl(pyridine-2-yl)methyl)benzene-1,2-diamine(0.273 g, 1.0 mmol) and 2-hydroxy-1-naphthaldehyde (0.172 g, 1.0 mmol) in MeOH (15 ml) for 12 hours at room temperature

Table 2. Estimation of the amount of Al^{3+} ions in industrial wastewater using HL

Sample	S. No.	Emission Intensity at 502 nm (a.u.)	The Concentration of Reference Required (mM)	The Concentration of Industrial Wastewater Required (mM)	Ratio of Reference concentration: Sample waste water concentration	Amount of Al^{3+} ions (mM)
Industrial wastewater	1	64	70.12	26.75	2.621	0.381
Industrial wastewater	2	45	103.73	38.65	2.683	0.372

yielded 1-(1-(Phenyl(pyridine-2-yl)methyl)-1H-benzo[d]imidazol-2-yl)naphthalene-2-ol. When irradiated at 400 nm, the probe was effectively employed as a “turn-on” fluorescence chemosensor to Al³⁺ion in the presence of a large number of other metal ions, and displays high strong blue emission (λ_{em} , 502 nm). The probe’s limit of detection (LOD) for Al³⁺is 3.3 nM. Mass spectrum analysis, job plot, and ¹H NMR measurements were used to determine the 1:1 metal-to-ligand complex. The pharmaceutical company effluent contains 0.38 mM of Al ion concentration at 64 emission intensity, which is significantly less than the WHO standard of 7.41 mM. The probe may also be used to detect Al³⁺ions in living cells (Hep G2). By fluorescence cell imaging processes, HL becomes a flexible sensor for identifying intracellular Al³⁺in human liver cancer cell line Hep G2 and human lung fibroblast cell lines, and the probe’s non-toxicity has been validated by MTT test up to 100 μM. All tests were conducted at ambient temperature.

Future Recommendations

The following research suggestions were well-received and can be utilized in future studies.

- In order to provide reliable data on the incidence of Al in industrial effluent, a more complete examination of a number of additional samples from diverse enterprises is necessary.
- Using DFT energy computations of the probe and the metal complex, the crystal structure of the ligand and the complex, including their HOMO-LUMO transitions, must be examined in detail.
- The crystal structure is critical, and it should be fully investigated while considering the metal and ligand coordination efficiency.
- When the chemical shift values of aromatic compounds are close together, it is difficult to distinguish the proton NMR signal peaks. As a result, the proton signal peaks should be widened and more easily distinguishable.
- The solid-state fluorescence experiment must be completed before the probes be used as light emitting diodes.

Acknowledgements

The authors would like to thank the faculties working in Materials Science and Engineering Department, Jimma University, Jimma, Ethiopia, for providing support to complete the MSc thesis. The authors confirm that no funding was received to conduct this study.

Ethical issues

The authors certify that this manuscript is the original work of the authors, all data collected during the study are presented in this manuscript, and no data from the study has been or will be published elsewhere separately.

Competing interests

The authors declare that they have no competing interests.

Authors' contributions

All authors contributed to the structure, content, and writing of the paper. The final version of the manuscript was reviewed, read, confirmed, and approved by all authors.

References

1. Berthon G. Aluminum speciation in relation to aluminum bioavailability, metabolism and toxicity. *Coord Chem Rev* 2002; 228(2): 319-41. doi: 10.1016/S0010-8545(02)00021-8.
2. Panhwar AH, Kazi TG, Afzadi HI, Abbasi AR, Arain MB, Arain SA, et al. Ultrasonic-assisted ionic liquid-based microextraction for preconcentration and determination of aluminum in drinking water, blood and urine samples of kidney failure patients: A multivariate study. *Analytical Methods* 2014; 6(20): 8277-83. doi: 10.1039/C4AY01735H.
3. World Health Organization. Guidelines for drinking-water quality: volume 1: recommendations, World Health Organization 1993; 2nd ed. Available from: <https://apps.who.int/iris/handle/10665/259956>
4. Reiber SH, Kukull W, Standish-Lee P. Drinking water aluminum and bioavailability. *Journal of the American Water Works Association* 1995; 87(5): doi. <https://doi.org/10.1002/j.1551-8833.1995.tb06367.x>
5. Alfrey AC, LeGendre GR, Kaehny WD. The dialysis encephalopathy syndrome. Possible aluminum intoxication. *N Engl J Med* 1976; 294(4): 184-8. doi: 10.1056/NEJM197601222940402.
6. Rondeau V, Commenges D, Jacqmin-Gadda H, Dartigues JF. Relation between aluminum concentrations in drinking water and Alzheimer's disease: An 8-year follow-up study. *Am J Epidemiol* 2000; 152(1): 59-66. doi: 10.1093/aje/152.1.59.
7. Martyn CN, Coggon DN, Inskip H, Lacey RF, Young WF. Aluminum concentrations in drinking water and risk of Alzheimer's disease. *Epidemiology* 1997; 8(3): 281-6. doi: 10.1097/00001648-199705000-00009.
8. Miller RG, Kopfler FC, Kelty KC, Stober JA, Ulmer NS. The occurrence of aluminum in drinking water. *American Water Works Association* 1984; 76(1): 84-91. doi: 10.1002/j.1551-8833.1984.tb05267.x.
9. Gauthier E, Fortier I, Courchesne F, Pepin P, Mortimer J, Gauvreau D. Aluminum forms in drinking water and risk of Alzheimer's disease. *Environ Res* 2000; 84(3): 234-46. doi: 10.1006/enrs.2000.4101.
10. Wettstein A, Aepli J, Gautschi K, Peters M. Failure to find a relationship between mnemonic skills of octogenarians and aluminum in drinking water. *Int Arch Occup Environ Health* 1991; 63(2): 97-103. doi: 10.1007/BF00379071.
11. McLachlan DR, Bergeron C, Smith JE, Boomer D, Rifat SL. Risk for neuropathologically confirmed Alzheimer's disease and residual aluminum in municipal drinking water employing weighted residential histories. *Neurology* 1996; 46(2): 401-5. doi: 10.1212/wnl.46.2.401.
12. Chen CH, Liao DJ, Wan CF, Wu AT. A turn-on and reversible Schiff base fluorescence sensor for Al³⁺ion. *Analyst* 2013; 138(9): 2527-30. doi: 10.1039/c3an00004d.
13. Campbell A, Becaria A, Lahiri DK, Sharman K, Bondy SC. Chronic exposure to aluminum in drinking water increases inflammatory parameters selectively in the brain. *J Neurosci Res* 2004; 75(4): 565-72. doi: 10.1002/jnr.10877.
14. Schintu M, Meloni P, Contu A. Aluminum fractions in drinking water from reservoirs. *Ecotoxicology and Environmental Safety* 2000; 46(1): 29-33. doi: 10.1006/eesa.1999.1887.

15. Akbari H, Soleimani H, Radford M, Biglari H, Faraji H, Nabavi S, et al. Data on aluminum concentration in drinking water distribution network of rural water supply in Sistan and Baluchistan province, Iran. *Data in Brief* 2018; 20: 1804-9. doi: 10.1016/j.dib.2018.08.180.
16. Zhang Y, Shi B, Zhao Y, Yan M, Lytle DA, Wang D. Deposition behavior of residual aluminum in drinking water distribution system: Effect of aluminum speciation. *Journal of Environmental Sciences* 2016; 42: 142-51. doi: 10.1016/j.jes.2015.05.010.
17. Klotz K, Weistenhofer W, Neff F, Hartwig A, van Thriel C, Drexler H. The health effects of aluminum exposure. *Dtsch Arztebl Int* 2017; 114(39): 653-659. doi: 10.3238/arztebl.2017.0653.
18. Panhwar AH, Kazi TG, Afzadi HI, Arain SA, Arain MS, Brahaman KD, Naeemullah, Arain SS. Correlation of cadmium and aluminum in blood samples of kidney disorder patients with drinking water and tobacco smoking: Related health risk. *Environ Geochem Health* 2016; 38(1): 265-74. doi: 10.1007/s10653-015-9715-y.
19. Wasana HM, Perera GD, De Gunawardena PS, Bandara J. The impact of aluminum, fluoride, and aluminum-fluoride complexes in drinking water on chronic kidney disease. *Environ Sci Pollut Res Int* 2015; 22(14): 11001-9. doi: 10.1007/s11356-015-4324-y.
20. Ganvir V, Das K. Removal of fluoride from drinking water using aluminum hydroxide coated rice husk ash. *J Hazard Mater* 2011; 185(2-3): 1287-94. doi: 10.1016/j.jhazmat.2010.10.044.
21. Van Dyke N, Yenugadhati N, Birkett NJ, Lindsay J, Turner MC, Willhite CC, Krewski D. Association between aluminum in drinking water and incident Alzheimer's disease in the Canadian Study of Health and Aging cohort. *Neurotoxicology* 2021; 83: 157-165. doi: 10.1016/j.neuro.2020.04.002.
22. Wang W, Yang H, Wang X, Jiang J, Zhu W. Factors effecting aluminum speciation in drinking water by laboratory research. *J Environ Sci (China)* 2010; 22(1): 47-55. doi: 10.1016/s1001-0742(09)60073-5.
23. Kimura M, Matsui Y, Kondo K, Ishikawa TB, Matsushita T, Shirasaki N. Minimizing residual aluminum concentration in treated water by tailoring properties of polyaluminum coagulants. *Water Research* 2013; 47(6): 2075-84. doi: 10.1016/j.watres.2013.01.037.
24. Willhite CC, Ball GL, McLellan CJ. Total allowable concentrations of monomeric inorganic aluminum and hydrated aluminum silicates in drinking water. *Crit Rev Toxicol* 2012; 42(5): 358-442. doi: 10.3109/10408444.2012.674101.
25. Becaria A, Campbell A, Bondy SC. Aluminum as a toxicant. *Toxicol Ind Health* 2002; 18(7): 309-20. doi: 10.1191/0748233702th157oa.
26. Pharmaceutical industry analysis report. Korea Health Industry Development Institute. Chungbuk. 2016; 5-41. [Cited 2017] Available from: https://scholar.google.com/scholar_lookup?title=Pharmaceutical+Industry+Analysis+Report.&publication_year=2017
27. Son HJ, Jang SH. Occurrence of residual pharmaceuticals and fate, residue and toxic effect in drinking water resources. *J Korean Soc Environ Eng* 2011; 33(6): 453-479. doi: 10.4491/KSEE.2011.33.6.453.
28. Heberer T. Occurrence, fate, and removal of pharmaceutical residues in the aquatic environment: A review of recent research data. *Toxicol Lett* 2002; 131(1-2): 5-17. doi: 10.1016/s0378-4274(02)00041-3.
29. Fent K, Weston AA, Caminada D. Ecotoxicology of human pharmaceuticals. *Aquat Toxicol* 2006; 76(2): 122-59. doi: 10.1016/j.aquatox.2005.09.009.
30. Korea Pharmaceutical Industry Guide. Korea Pharmaceutical and Bio-Pharma Manufacturers Association. 2017; 125-138. [Cited 2017]. Available from: <https://www.kpbma.or.kr/english/globalization>
31. Malakootian M, Pournamdar M, Asadipour A, Mahdizadeh H. Degradation and removal of p-nitroaniline from aqueous solutions using a novel semi-fluid Fe/charcoal micro-electrolysis reactor. *Korean J Chem Eng* 2019; 36(2): 217-25. doi: 10.1007/s11814-018-0166-x.
32. Khodadadi M, Mesdaghinia A, Nasseri S, Ghaneian MT, Ehrampoush MH, Hadi M. Prediction of the waste stabilization pond performance using linear multiple regression and multi-layer perceptron neural network: A case study of Birjand, Iran. *Environmental Health Engineering and Management Journal* 2016; 3(2): 81-9. doi: 10.15171/EHEM.2016.05.
33. Barbooti MM. Role of organic matter, clay, and iron contents in the sorption of oxytetracycline on river sediments. *Environ Health Eng Manag* 2017; 4(2): 109-15. doi: 10.15171/EHEM.2017.15.
34. Malakootian M, Mahdizadeh H, Khavari M, Nasiri A, Gharaghani MA, Khatami M, Sahle-Demessie E, Varma RS. Efficiency of novel Fe/charcoal/ultrasonic micro-electrolysis strategy in the removal of Acid Red 18 from aqueous solutions. *Journal of Environmental Chemical Engineering* 2020; 8(2): 103553-7. doi: 10.1016/j.jece.2019.103553.
35. Amirmahani N, Mahdizadeh H, Malakootian M, Pardakhty A, Mahmoodi NO. Evaluating nanoparticles decorated on $\text{Fe}_3\text{O}_4@\text{SiO}_2$ -schiff base ($\text{Fe}_3\text{O}_4@\text{SiO}_2$ -APTMS-HBA) in adsorption of ciprofloxacin from aqueous environments. *Journal of Inorganic and Organometallic Polymers and Materials* 2020; 30: 3540-3551. doi: 10.1007/s10904-020-01499-5.
36. Chaudhuri S, Bera S, Biswas MK, Roy AS, Weyhermuller T, Ghosh P. Oxidovanadium(IV), Oxidomolybdenum(VI) and cobalt (III) complexes of o-phenylenediamine derivatives: Oxidative dehydrogenation and photoluminescence. *Inorg Chem Front* 2014; 1(4): 331-41. doi: 10.1039/C3QI00103B.
37. Maiti D, Islam AS, Sasmal M, Prodhan C, Ali M. Selective sensing of nitric oxide by a 9, 10-phenanthroquinone-pyridoxal based fluorophore. *Photoch Photobio Sci* 2018; 17(9): 1213-21. doi: 10.1039/C8PP00115D.
38. Nakashima Y, Nahar S, Miyagi-Shiohira C, Kinjo T, Kobayashi N, Saitoh I, Watanabe M, Fujita J, Noguchi H. A Liquid Chromatography with Tandem Mass Spectrometry-Based Proteomic Analysis of Cells Cultured in DMEM 10% FBS and Chemically Defined Medium Using Human Adipose-Derived Mesenchymal Stem Cells. *Int J Mol Sci* 2018; 19(7): 2042. doi: 10.3390/ijms19072042.
39. Samui A, Pal K, Karmakar P, Sahu SK. In situ synthesized lactobionic acid conjugated NMOFs, a smart material for imaging and targeted drug delivery in hepatocellular carcinoma. *Mat Sci ENG C* 2019; 98: 772-81. doi: 10.1016/j.msec.2019.01.032.
40. Hens A. A turn off and reversible fluorescence probe (HNAPP) for Zn (II) ion towards inorganic phosphate ions (H_2P and HP) at physiological pH. *RSC Adv* 2015; 5(67): 54352-54363. doi: 10.1039/C5RA07613G.
41. Wu D, Sedgwick AC, Gunnlaugsson T, Akkaya EU, Yoon J, James TD. Fluorescent chemosensors: The past, present and future. *Chem Soc Rev* 2017; 46(23): 7105-23. doi: 10.1039/C7CS00240H.